crystals

MDPI

Article

Embracing $[XY_3]^{m-}$ and $[XY_4]^{m-}$ Anions in Salts of $[M(bpy)_3]^{q+}$

Edwin C. Constable * and Catherine E. Housecroft

Department of Chemistry, University of Basel, BPR 1096, Mattenstrasse 22, Postfach, 4002 Basel, Switzerland
* Correspondence: edwin.constable@unibas.ch

Abstract: $[M(bpy)_3]^{q+}$ cations (bpy = 2,2′-bipyridine) are archetypical coordination entities containing chelating bidentate *N*,*N*′-donor ligands. Each propeller-shaped cation is chiral, existing as a Δ or Λ enantiomer. The supramolecular chemistry of $[M(bpy)_3]^{q+}$ cations in the crystal is dominated by cation-anion interactions and, to a lesser extent, weaker non-covalent interactions. Analysis of the data for $[M(bpy)_3]^{q+}$ salts in the Cambridge Structural Database (CSD) reveals a ubiquitous motif in which homochiral sheets of cations generate cavities for the accommodation of anions. A series of related and common motifs in the solid-state structures of $[M(bpy)_3]^{q+}$ salts has been identified. One of the commonest motifs comprises a hexagon of six cations with anions either in the center or lying above and/or below the centroid.

Keywords: metal complexes; 2,2′-bipyridine; $[M(bpy)_3]^{q+}$; $[XY_n]^{m-}$ anion; C–H…Y interactions; chirality

1. Introduction

One hundred and thirty-five years after its birth [1,2], 2,2′-bipyridine (Scheme 1, bpy), the "most widely used ligand" [3], remains a key weapon in the arsenal of the coordination chemist [4–12]. Although best known as a chelating, bidentate *N*,*N*′-donor, bpy continues to delight and intrigue us with new twists and turns in its chemistry. Unusual bonding modes include monodentate, bridging and cyclometallated coordination and the established reactivity patterns include ligand-centered as well as metal-centered processes [13,14]. Furthermore, many "simple" compounds containing bpy and related ligands have been shown to be comprised of coordination polymers or networks in the solid state [15]. 2,2′-Bipyridine and related metal-binding domains have played a key role in the development of supramolecular and metallosupramolecular chemistry.

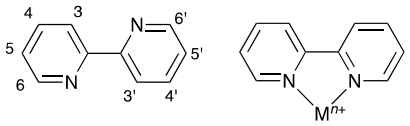

Scheme 1. Structure of bpy showing the change in conformation upon metal coordination. The atom numbering is also defined.

Although the use of the bpy metal-binding domains in supramolecular chemistry is well-established, the supramolecular chemistry of simple complexes containing bpy and related ligands is less studied. Dance has established the importance of "embraces" involving interactions between aromatic rings in the packing of complexes containing bpy ligands [16–19]. Although multifold van der Waals interactions and weak hydrogen bonding can result in dominant packing forces in the assembly of crystalline solids, electrostatic interactions are expected to be an order of magnitude stronger.

We have recently shown that a dominant motif in the solid-state structures of $[M(bpy)_3]^{q+}$ salts containing halide anions is the "halide embrace" (Figure 1) in which six

Citation: Constable, E.C.; Housecroft, C.E. Embracing $[XY_3]^{m-}$ and $[XY_4]^{m-}$ Anions in Salts of $[M(bpy)_3]^{q+}$. *Crystals* **2023**, *13*, 97. https://doi.org/10.3390/cryst13010097

Academic Editor: Leonid Kustov

Received: 24 December 2022
Revised: 2 January 2023
Accepted: 3 January 2023
Published: 5 January 2023

homochiral $[M(bpy)_3]^{q+}$ cations surround a halide anion [20]. Our initial studies were predicated upon the importance of short contacts with H3 and H3′ of the bpy ligands; however, we subsequently recognized that these interactions were part of a broader supramolecular chemistry in the crystals containing $[M(bpy)_3]^{q+}$ cations. In this paper, we describe further studies on the influence of cation…anion interactions on the solid-state packing of $[M(bpy)_3]^{q+}$ salts and identify a number of common embraces involving polyatomic anions $[XY_n]^{m-}$. The structural data for this article were retrieved from the Cambridge Structural Database (CSD) [21] (see Section 2).

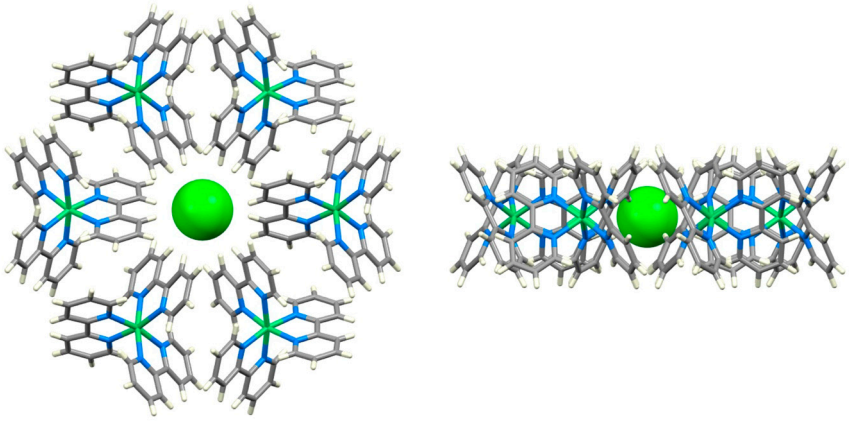

Figure 1. The halide embrace exemplified with the motif observed in $[Ni(bpy)_3]Cl_2{\cdot}5.5H_2O$, CSD refcode EGOVEB [22]. (**a**) The Cl^- ion at the center of a motif of six homochiral $[Ni(bpy)_3]^{2+}$ cations, and (**b**) a side view of the same motif; this unit is part of a 2D-sheet.

2. Methods

Conquest (version 2022.3.0 including November 2022 updates) [23] was used to search the CSD [21] for the $[M(bpy)_3]$ motif (M = any transition metal; substituted bpy ligands were excluded by explicit inclusion of C-bonded hydrogen atoms) combined with XY_3, XY_4 or XY_5 units in which X and Y are any atom, and the X–Y bond was of 'any type'. The connectivities of the X atoms were constrained to three, four or five respectively, and the number of bonded atoms for Y was constrained to one.

Analysis of structures was carried out using the program Mercury (version 2022.3.0) [24]. In cases where H atom coordinates were not available, H positions were added in Mercury [24]. All H positions were normalized within Mercury, such that all C–H bond lengths were 1.089 Å. The settings in Mercury for a 'short contact' (sum of the van der Waals radii + 0.1 Å) were applied to locate H...Y interactions.

Disordered structures were retained in the analysis. Since disorders often involve the $[XY_n]^{m-}$ anions, the contact distances in the discussion are given as ranges for individual compounds, and C–H...X distances are also given since the position of the central atom X is typically unambiguously defined.

3. Defining the Sets of Structures for Analysis

An initial search for the $[M(bpy)_3]$ motif with no constraints on charge or counterion yielded 701 hits. Adding a separate XY_3 motif gave 25 hits, six of which contained the $[H_3O]^+$ ion as the XY_3 species (CSD refcodes CINYUV, DIFYUO, JARWOP, QUMCIM, QUMCOS, and TIMYEW). These were excluded from further analysis. Of the 19 remaining, three contained additional molecular motifs which impacted significantly on the crystal packing: $[Ni(bpy)_3][UO_2(H_2L)(H_2O)]_2[NO_3]_2{\cdot}3H_2O$ (refcode CUFPUO, H_4L = 1,1′-biphenyl-2,2′,6,6′-tetracarboxylic acid) [25], a guanidinium organosulfonate host containing $[Ru(bpy)_3]^{2+}$ with formate ions as the $[XY_3]^-$ species (refcode RUPGAN) [26], $[Rh(bpy)_3][Pt(NO_3)_6][NO_3]{\cdot}Me_2CO{\cdot}MeCN{\cdot}H_2O$ (refcode QUDXIZ) [27]. Two structures

from the XY_3 search contain both $[NO_3]^-$ and $[CrO_4]^{2-}$ ions (refcodes EHIHUY [28] and XUJDEL [29]) and fall into the discussion of $[XY_4]^{m-}$ ions in terms of packing motifs. For $[Ni(bpy)_3][NO_3]_2{\cdot}5H_2O$ (refcode ZZZVRW), no atomic coordinates are available in the CSD [30]. This gave a data set for $[M(bpy)_3]$ with $[XY_3]^{m-}$ of 13 entries for detailed discussion (see Section 5), which reduces to 12 structures as one hit corresponded to a space group correction for the CSD entry VATHIJ [31].

A search which combined the $[M(bpy)_3]$ motif with an XY_4 unit resulted in 82 hits. Five contained $[NH_4]^+$ as the XY_4 motif (refcodes ELIXOP, OMUHIP, QEKCUH, QEKDAO, QEKDES), and three contained either $CHCl_3$ or CH_2Cl_2 as XY_4 (refcodes MOMXAO, SACDOQ, SACDIK). These were omitted from further analysis. Eleven structures were excluded based on the fact that additional molecular entities appreciably affected the crystal packing, or that the $[M(bpy)_3]^{2+}$ ions were embedded in an $[M_2(ox)_3]_n^{n-}$ metal-organic framework: $[Fe(bpy)_3][SO_4{\subset}L]{\cdot}9H_2O$, in which the sulfate ion is encapsulated in a tris(3-pyridylurea) receptor, L (refcode BULLEA) [32], $[Co(bpy)_3]_2[L'][ClO_4]{\cdot}4H_2O$ where $[L']^{5-}$ is a 4-sulfonatothiacalix [4]arene derivative (refcode NARWEJ) [33], $Na[Fe(bpy)_3]_2[Fe_2Sr_2Mo_{12}O_{24}(OH)_6(H_2O)_8(H_2PO_4)_2(HPO_4)_2(PO_4)_4][PO_4]{\cdot}9H_2O$ (refcode RAXBAV) [34], $[Mn_{32}(thme)_{16}(bpy)_{24}(N_3)_{12}(OAc)_{12}][Mn(bpy)_3]_{1.5}[ClO_4]_{11}{\cdot}11.5MeCN{\cdot}12H_2O$ (H_3thme = 1,1,1-tris(hydroxymethyl)ethane, TAXHEG) [35], (n\{$[Ru(bpy)_3][ClO_4]$\})$[MnCr(ox)_3]_n$ (refcodes GUNFAW, GUNFAW01) [36,37], (n\{$[Co(bpy)_3][ClO_4]$\})$[Co_2(ox)_3]_n$ (refcode PIMYUF) [38], (n\{$[Cr(bpy)_3][ClO_4]$\})$[NaCr(ox)_3]_n$ (refcode ZUQVAI), (n\{$[Cr(bpy)_3][ClO_4]$\})$[Mn_2(ox)_3]_n$ (refcode ZUQVEM) and (n\{$[Cr(bpy)_3][BF_4]$\})$[Mn_2(ox)_3]_n$ (refcode ZUQVIQ) [39]. For $[Re(bpy)_3][ReO_4]_2$ (refcode FEZLOL [40]), atomic coordinates for the Re and O atoms are not available in the CSD, and no coordinates can be accessed for the structure with refcode OFAYIF, although clearly, the $[PO_4]$-unit is part of a Keggin-polyoxomolybdate cage and is therefore not relevant to the present study [41]. Coordinates for $[Ni(bpy)_3][SO_4]{\cdot}7H_2O$ (refcode ZZZKFE) [42] are also not available. The final data set for structural analysis of $[M(bpy)_3]^{q+}$ combined with $[XY_4]^{m-}$ was comprised of 61 structures, including several redeterminations (see Section 6).

We note that a search for the $[M(bpy)_3]$ motif with an XY_5 unit revealed no examples of this combination.

4. An Aside on Chirality

Chirality in inorganic systems is a topic dividing the community between those for whom it is a nightmare and those who embrace its elegance and beauty. Unfortunately for the former group, discussions of the spatial properties of $[M(bpy)_3]^{q+}$ must also consider their inherent chirality. An object is chiral if the object and its mirror image are not identical and cannot be superposed (the IUPAC uses the word superpose rather than the more familiar English word superimpose) [43]. To be chiral, a molecule must have no mirror planes, no centers of inversion or rotation–reflection axes. Any one of these symmetry elements present in a molecule will preclude chirality and achiral objects possess a mirror plane, a center of inversion, or a rotation–reflection axis [44].

$[M(bpy)_3]$ coordination entities are chiral and may exist as one of two enantiomers (mirror images). The absolute configuration may be denoted by the stereochemical descriptors Δ and Λ (Figure 2) [45]. These descriptors are more convenient and easier to visualise than the more general configuration index [45] and refer to a readily identifiable screw axis (Figure 2).

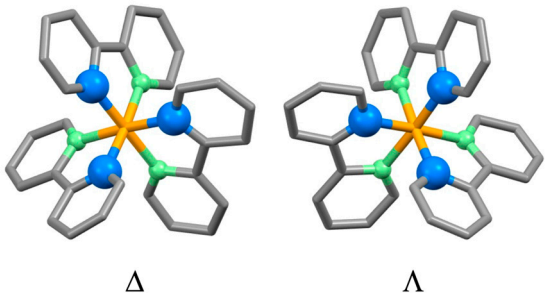

Figure 2. The absolute configuration of the enantiomers of an [M(bpy)$_3$] coordination moiety is conveniently denoted by the stereochemical descriptors Δ and Λ. In each bpy ligand, the green atoms are further away from the observer and the blue atoms are closer and can be related to an axis orthogonal to the plane of the paper and running through the metal center. An anti-clockwise rotation of the right-hand structure about this axis will "dig" the propeller into the page and this is described as the Λ-enantiomer. The mirror-image propeller on the left must be rotated clockwise about the axis to screw into the page and is denoted as the Δ-enantiomer.

5. [M(bpy)$_3$]$^{q+}$ Combined with [XY$_3$]$^{m-}$

Of the 13 structures in the data set of [M(bpy)$_3$]$^{q+}$ combined with [XY$_3$]$^{m-}$, 12 involve nitrate ions and one features a sulfite ion. The latter appears in [Fe(bpy)$_3$]$_2$[SO$_3$][OH]$_4$·14H$_2$O (refcode YAWWAY) [46] and provides our first example of an [XY$_3$]$^{m-}$ ion interacting with six [M(bpy)$_3$]$^{q+}$ cations in the hexagonal motif shown in Figure 3. This defines what we call the Type 1 structural motif. The solid-state structure of [Fe(bpy)$_3$]$_2$[SO$_3$][OH]$_4$·14H$_2$O comprises [Fe(bpy)$_3$]$^{3+}$ cations assembled into layers separated by sheets of hydrogen-bonded [OH]$^-$ ions and H$_2$O molecules. The monoclinic space group *C*2/*c* requires that equal numbers of (Δ)- and (Λ)-[Fe(bpy)$_3$]$^{3+}$ are present, and they assemble into alternating homochiral sheets. Just as in the halide embraces that we have previously described [20], this results in each Type I motif consisting of six (Λ)-[Fe(bpy)$_3$]$^{3+}$ or six (Δ)-[Fe(bpy)$_3$]$^{3+}$ cations. Figure 3a,b show orthogonal views of the Type I motif. The twelve bpy H3 and H3′ atoms point towards the [SO$_3$]$^{2-}$ ion, and the CH...O and C...S metrics are given in Table 1. As noted in Section 2, we have chosen to include the distance from the C to the central atom of the [XY$_n$]$^{m-}$ ion because, in many cases, the anions discussed in this article suffer from a disorder of the Y atoms about common X positions.

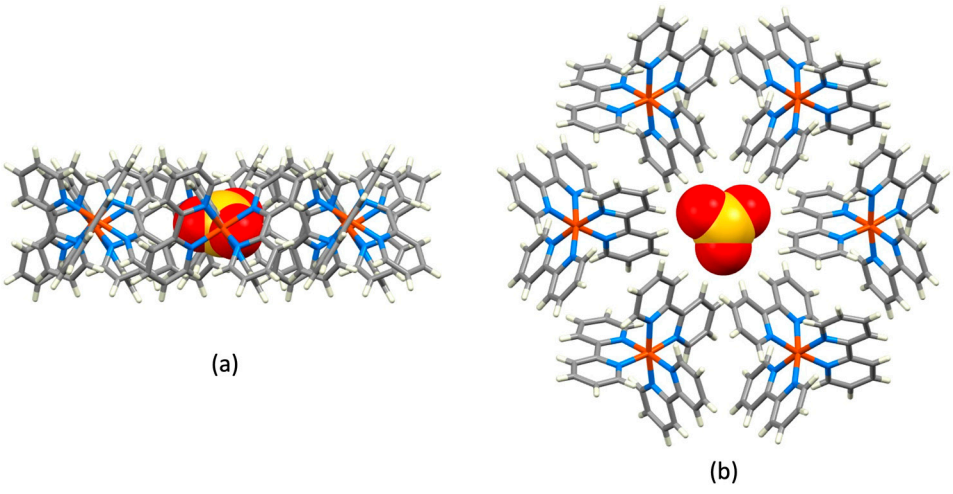

Figure 3. Structure Type I illustrated with the motif found in [Fe(bpy)$_3$]$_2$[SO$_3$][OH]$_4$·14H$_2$O which possesses a sheet structure (refcode YAWWAY) [46]. (**a**) One hexagonal motif within one sheet viewed down the crystallographic *a*-axis, and (**b**) the same unit viewed from above showing the twelve bpy H3 and H3′ atoms oriented towards the [SO$_3$]$^{2-}$ ion.

The motif shown in Figure 3b extends into the 2D sheet displayed in Figure 4, such that all H3 and H3′ atoms (shown in red in Figure 4) of the three bpy ligands in an $[Fe(bpy)_3]^{2+}$ cation are directed into a 'hole' in the sheet (Figure 4a) and are available to interact with a hosted anion. The side view of part of one sheet in Figure 4b illustrates that the H3 and H3′ atoms lie within the sheet while the H4, H5, H6, H4′, H5′ and H6′ atoms are located on the top and bottom surfaces of the sheet.

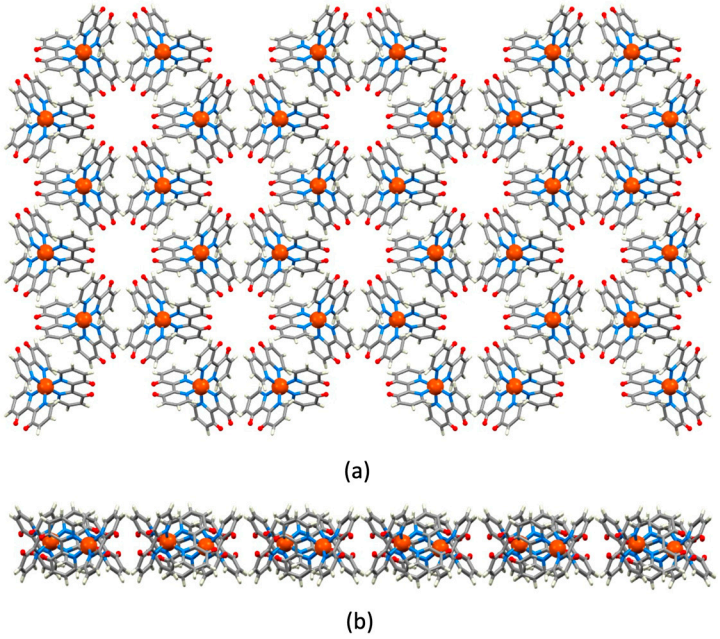

Figure 4. (**a**) Part of one sheet comprising (Δ)-$[Fe(bpy)_3]^{2+}$ cations in $[Fe(bpy)_3]_2[SO_3][OH]_4{\cdot}14H_2O$ (refcode YAWWAY [46]) with $[SO_3]^{2-}$, $[OH]^-$ and H_2O omitted. (**b**) The same sheet section viewed from the side. The H3 and H3′ atoms are shown in red.

Table 1. Structure Type I and II complexes with $[XY_3]^{m-}$ anions.

REFCODE Space Group	X Y	Structure Type	Range H…Y/Å (Mean H…Y/Å)	Range C…Y/Å (Mean C…Y/Å)	Range ∠C–H…Y/° (Mean ∠C–H…Y/°)	Range C…X/Å (Mean C…X/Å)	Refs.
YAWWAY *C*2/*c*	S O	I	2.182–2.442 (2.296)	3.243–3.529 (3.370)	163.0–175.3 (169.2)	4.051–4.487 (4.270)	[46]
OLOCOI *C*2/*c*	N O	II	2.136–2.815 (2.477)	3.141–3.432 (3.286)	110.8–160.6 (133.0)	3.930–4.573 (4.158)	[47]
XARPEN *C*2/*c*	N O	II	2.230–2.786 (2.491)	3.247–3.534 (3.402)	117.6–160.1 (143.2)	3.836–4.532 (4.215)	[48]
YEJKOP *C*2/*c*	N O	II	2.212–2.781 (2.470)	3.234–3.518 (3.378)	117.6–159.2 (142.8)	3.818–4.598 (4.185)	[49]

The compound $[Zn(bpy)_3][NO_3][azt]_{0.5}{\cdot}6H_2O$ ($[azt]^{2-}$ = 5,5′-(diazene-1,2-diyl)bis(tetrazol-2-ide)) crystallizes in a sheet structure (refcode OLOCOI) with hydrogen-bonded $[azt]^{2-}$ and H_2O molecules forming layers between the sheets [47]. The $[Zn(bpy)_3]^{2+}$ ions in $[Zn(bpy)_3][NO_3][azt]_{0.5}{\cdot}6H_2O$ assemble into a homochiral sheet, analogous to that in $[Fe(bpy)_3]_2[SO_3][OH]_4{\cdot}14H_2O$, and alternating sheets contain (Δ)- or (Λ)-$[Zn(bpy)_3]^{2+}$ ions, respectively, consistent with the space group (Table 1). The $[NO_3]^-$ ions are located in pockets within the top and bottom surfaces of each sheet (Figure 5a). The range of CH...O, C...O and C...N distances and C–H...O angles, and the mean values are given in Table 1. We define this motif (Figure 5b) as Type II. It is also observed in the isostructural compounds $[Co(bpy)_3][NO_3]_2{\cdot}H_2O{\cdot}MeCN$ (XARPEN, Table 1) [48] and $[Ni(bpy)_3][NO_3]_2{\cdot}H_2O{\cdot}MeCN$ (YEJKOP, Table 1) [49]. In these Type II motifs, each $[NO_3]^-$

exhibits short contacts to H3 and H3′ atoms of six $[M(bpy)_3]^{2+}$ cations in addition to three O...H4 contacts (Figure 6).

The crystal structure of $[Co(bpy)_3]_2[Co(OH_2)_6][NO_3]_8{\cdot}7H_2O$ (refcode VATHIJ and a later entry VATHIJ01 which gives a revised space group of *P*2/*c*) also reveals the encapsulation of $[NO_3]^-$ ions within $[Co(bpy)_3]_n^{2n+}$ sheets [31,50]. However, in this case, each sheet is heterochiral, and the hexagonal motifs are absent.

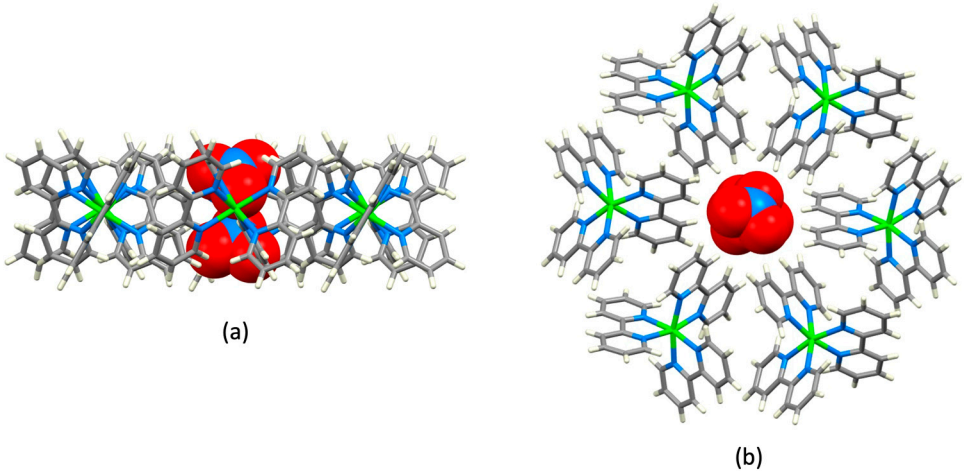

Figure 5. Structure Type II illustrated with the motif found in $[Zn(bpy)_3][NO_3][azt]_{0.5}{\cdot}6H_2O$ which possesses a sheet structure (refcode OLOCOI) [47]. (**a**) One hexagonal motif which hosts two $[NO_3]^-$ ions, and (**b**) the same unit viewed from above.

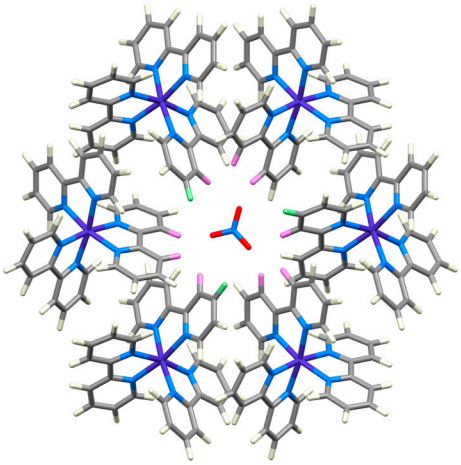

Figure 6. Packing motif in $[Co(bpy)_3][NO_3]_2{\cdot}H_2O{\cdot}MeCN$ (CSD refcode XARPEN [48]); the second symmetry-related $[NO_3]^-$ is omitted for clarity. The H3 and H3′ atoms in the bpy ligand which show short contacts to the $[NO_3]^-$ ion are shown in pink and H4 atoms in green.

The structure of $[Ni(bpy)_3]_2[NO_3]_3[1\text{-}CO_2H\text{-}2\text{-}CO_2C_6H_4]{\cdot}4H_2O$ (refcode PUGTEQ, monoclinic space group *Cc*) [51] also consists of alternating (Δ)- and (Λ)-homochiral sheets of $[Ni(bpy)_3]^{2+}$ cations, assembled with the hexagonal motifs described in Figure 4. However, the cavities in these sheets remain vacant. Instead, the $[NO_3]^-$ ions are involved in hydrogen-bonded networks with hydrogen phthalate ions and water molecules, each 2D network being sandwiched between the $[Ni(bpy)_3]_n^{2n+}$ sheets. We attribute this structural preference to the presence of the hydrogen phthalate ion which can act as both a strong hydrogen-bond donor and acceptor. $[Ni(bpy)_3]_2[NO_3]_3[1\text{-}CO_2H\text{-}2\text{-}SO_3C_6H_4]{\cdot}9H_2O$ (refcode OGUNAG [52]) is related to $[Ni(bpy)_3]_2[NO_3]_3[1\text{-}CO_2H\text{-}2\text{-}CO_2C_6H_4]{\cdot}4H_2O$, and also exhibits hexagonal motifs of $[Ni(bpy)_3]^{2+}$ cations forming (Δ)- and (Λ)-homochiral sheets

separated by 2D-hydrogen bonded nets comprising 3-carboxybenzenesulfonate anions, nitrate ions and water molecules. However, in this case, $[NO_3]^-$ ions are also hosted within the $[Ni(bpy)_3]_n^{2n+}$ sheets (Figure 7), but only half the number as seen in the Type II motif. The $[NO_3]^-$ ion engages in six short contacts with H3 and H3′ of four bpy ligands and two short O...H4 contacts, and we designate this as a Type III structure. Metrics for the contacts are given in Table 2. The location of the nitrate ions in the crystal lattice of $[Ni(bpy)_3]_2[NO_3]_3[1\text{-}CO_2H\text{-}2\text{-}SO_3C_6H_4]\cdot 9H_2O$ again suggests that the presence of a strong hydrogen bond donor/acceptor can redirect the assembly of the Type II assembly, effectively 'pulling' the nitrate ion out of the $[Ni(bpy)_3]_n^{2n+}$ sheet into the hydrogen-bonded network.

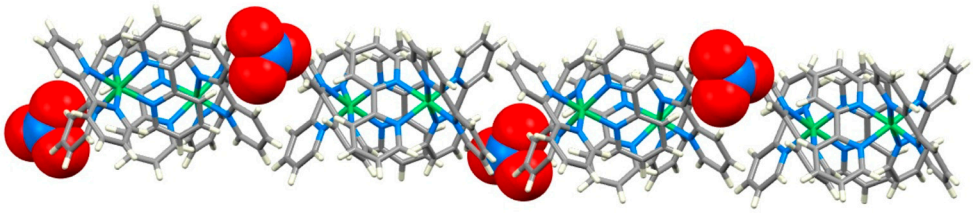

Figure 7. Structure Type III: A side view of part of one $[Ni(bpy)_3]_n^{2n+}$ sheet hosting $[NO_3]^-$ anions in $[Ni(bpy)_3]_2[NO_3]_3[1\text{-}CO_2H\text{-}2\text{-}SO_3C_6H_4]\cdot 9H_2O$ (refcode OGUNAG [52]). H_2O molecules, which also contact CH units in the sheet, are omitted for clarity.

Table 2. Structure Type III complex with $[NO_3]^-$ anions.

REFCODE Space Group	X Y	Structure Type	Range H…Y/Å (Mean H…Y/Å)	Range C…Y/Å (Mean C…Y/Å)	Range ∠C–H…Y/° (Mean ∠C–H…Y/°)	Range C…X/Å (Mean C…X/Å)	Ref.
OGUNAG $P2_1/n$	N O	III	2.369–2.813 (2.639)	3.418–3.766 (3.602)	127.0–174.9 (150.8)	3.631–4.851 (4.102)	[52]

The preference for the nitrate ion to be involved in a hydrogen-bonded assembly rather than be hosted within or adjacent to the $\{[M(bpy)_3]^{2+}\}_6$ motifs is also observed in the series of compounds $[Cu(bpy)_3]_2[Cr(ox)_3][NO_3]\cdot 9H_2O$ (refcode MELMUM, ox^{2-} = oxalate) [53], $[Ni(bpy)_3]_2[Cr(ox)_3][NO_3]\cdot 10H_2O$ (refcode QOYDEO) [54], $[Fe(bpy)_3]_2[Fe(ox)_3][NO_3]\cdot 10H_2O$ (refcodes WOMNIY, WOMNIY01) [55], and $[Cu(bpy)_3]_2[Fe(ox)_3][NO_3]\cdot 10H_2O$ (refcode WOMNUK) [55]. All feature layer structures with alternating homochiral-$[M(bpy)_3]_n^{2n+}$ layers (as shown in Figure 4) and hydrogen-bonded sheets comprising nitrate and $[M(ox)_3]^{3-}$ ions and water molecules. These were described by Jurić et al. as 'honeycomb like hydrophobic layers' with 'each hydrophobic layer sandwiched between two hydrophilic layers' [53]. Jurić et al. also point to the extensive C–H...O interactions at the interfaces of the sheets. Among these, the interactions between the O atoms of the $[M(ox)_3]^{3-}$ ion and the bpy H3, H3′ and H4 atoms, as well as to one H5 and one H6, are of note.

6. $[M(bpy)_3]^{q+}$ Combined with $[XY_4]^{m-}$

The 61 hits in the CSD with $[M(bpy)_3]^{q+}$ combined with $[XY_4]^{m-}$ reduced to 50 different structures, once structural redeterminations were accounted for. Analysis of the structural data showed that, with two exceptions, sulfate, thiosulfate, chromate, and molybdate salts (14 structures) conformed to a common pattern which resembled the Type II assembly described above for the nitrate salts (Figure 5 and Table 1). The exceptions, $[Zn(bpy)_3][CrO_4]_{0.5}[NO_3]\cdot 6.5H_2O$ [29] and $[Co(bpy)_3][CrO_4]_{0.5}[NO_3]\cdot 7H_2O$ [28] (refcodes XUJDEL and EHIHUY, respectively) adopt a Type I assembly. Thus, all 14 structures comprise alternating homochiral layers of (Δ)- or (Λ)-$[M(bpy)_3]^{2+}$ cations arranged in

hexagonal motifs. These sheets are interleaved with hydrogen-bonded networks involving water molecules, and, in two cases, nitrate ions (refcodes EHIHUY [28] and XUJDEL [29]). Figure 8a,b display the Type I motif in $[Zn(bpy)_3][CrO_4]_{0.5}[NO_3]\cdot 6.5H_2O$ [29]. There are 14 C–H...O contacts involving bpy H3 and H3′ atoms, and metrics for these interactions are given in Table 3, along with those for $[Co(bpy)_3][CrO_4]_{0.5}[NO_3]\cdot 7H_2O$. Figure 8c,d show the Type II motif in $[Cu(bpy)_3][SO_4]\cdot 7.5H_2O$ (refcode ROLLOU) [56]. The Type II motif also appears in $[Fe(bpy)_3][SO_4]\cdot 7.5H_2O$ (refcode MOSHUZ) [57], $[Co(bpy)_3][SO_4]\cdot 7.5H_2O$ (refcode KOKDUM) [58], $[Ni(bpy)_3][SO_4]\cdot 7.5H_2O$ (refcode BPYNIS) [59], $[Zn(bpy)_3][SO_4]\cdot 7.5H_2O$ (refcode OREHEZ) [60], $[Co(bpy)_3][SO_4]\cdot 8.5H_2O$ (refcode LIFDOV) [61], $[Ni(bpy)_3][SSO_3]\cdot 7H_2O$ (refcode KOLXOY) [62], $[Zn(bpy)_3][SSO_3]\cdot 7H_2O$ (refcode ROKHII) [63], $[Cu(bpy)_3][CrO_4]\cdot 7.5H_2O$ (refcode RUYYIU) [64], $[Zn(bpy)_3][CrO_4]\cdot 7.5H_2O$ (refcode NEMPAW) [65], $[Ni(bpy)_3][CrO_4]\cdot 7.5H_2O$ (refcode VADPUM) [66], and $[Ni(bpy)_3][MoO_4]\cdot 7.5H_2O$ (refcode ELIMUH) [67]. As with the Type II nitrate salts described in Section 5, the Type II $[XY_4]^{2-}$ anions show short contacts with bpy H3 and H4 atoms, with a dominance of H4 contacts; relevant distances and angles are summarized in Table 3. In the thiosulfate salts $[Ni(bpy)_3][SSO_3]\cdot 7H_2O$ and $[Zn(bpy)_3][SSO_3]\cdot 7H_2O$, the $[SSO_3]^{2-}$ ions are oriented with the O_3S–S vector pointing directly into the $\{[M(bpy)_3]\}_6$-motif (Figure 9). This facilitates six S...H3 contacts which are augmented by six O...H4 interactions (Table 3). Salts of $[M(bpy)_3]^{2+}$ containing $[SO_4]^{2-}$, $[SSO_3]^{2-}$, $[CrO_4]^{2-}$, and $[MoO_4]^{2-}$ anions, are therefore all classified into Type I or Type II structures, and it is interesting to note that the Type I structures also contain a nitrate ion accommodated in the hydrogen-bonded water layer. Wojciechowska et al. [29] commented that the presence of the $[NO_3]^-$ ion appears to be important for the stabilization of the crystal structure. Our survey of the Type I structures here and in the previous section shows that there is a tendency for $[NO_3]^-$ to prefer stronger hydrogen-bonded interactions with H_2O molecules in preference to multiple CH_{bpy}...O contacts.

While the hexagonal $\{[M(bpy)_3]\}_6$ motif is ubiquitous in the $[SO_4]^{2-}$, $[SSO_3]^{2-}$, $[CrO_4]^{2-}$, and $[MoO_4]^{2-}$ salts, the same is not true of perchlorate and tetrafluoridoborate salts. None of the three $[BF_4]^-$ salts (refcodes JIWTOZ, PAHNUI and RIGTEH) exhibits homochiral layers and hence lacks a packing motif that embraces the anion. Perchlorate salts account for 25 of the 51 structures containing $[M(bpy)_3]^{q+}$ cations combined with $[XY_4]^{m-}$ anions. A number of these compounds crystallize with additional molecular anions or cations (refcodes CEDXUG, BPBPFE, KIFWIF, QITBUT, VABJIU) or free bpy (refcodes DEZPII, ROJQAI) and, in each case, these additional species disrupt the assembly of $\{[M(bpy)_3]\}_6$ motifs. Although enantiomerically pure, (Λ)-$[Ru(bpy)_3][ClO_4]_2$ (refcode EWOTEQ, space group $P2_12_12_1$) [68] does not form $\{[Ru(bpy)_3]\}_6$ motifs and lacks the hydrogen-bonded sheets that typically separate homochiral layers in Type I, Type II and Type III classes. Other structures which do not exhibit homochiral layer structures of Types I, II and III are those with refcodes CEZMAV, FIXKUT, CUHVUW, JAQDIR, POMJUX, TBPYCU, TIBMAU, YOWHEX, and ZAMGAV03; the latter (crystallizing in space group $P\bar{1}$) is a polymorph of ZAMGAV (space group $C2/c$, see below). This leaves eight structures (32% of the perchlorate salts analyzed) with structural motifs of interest that are described below.

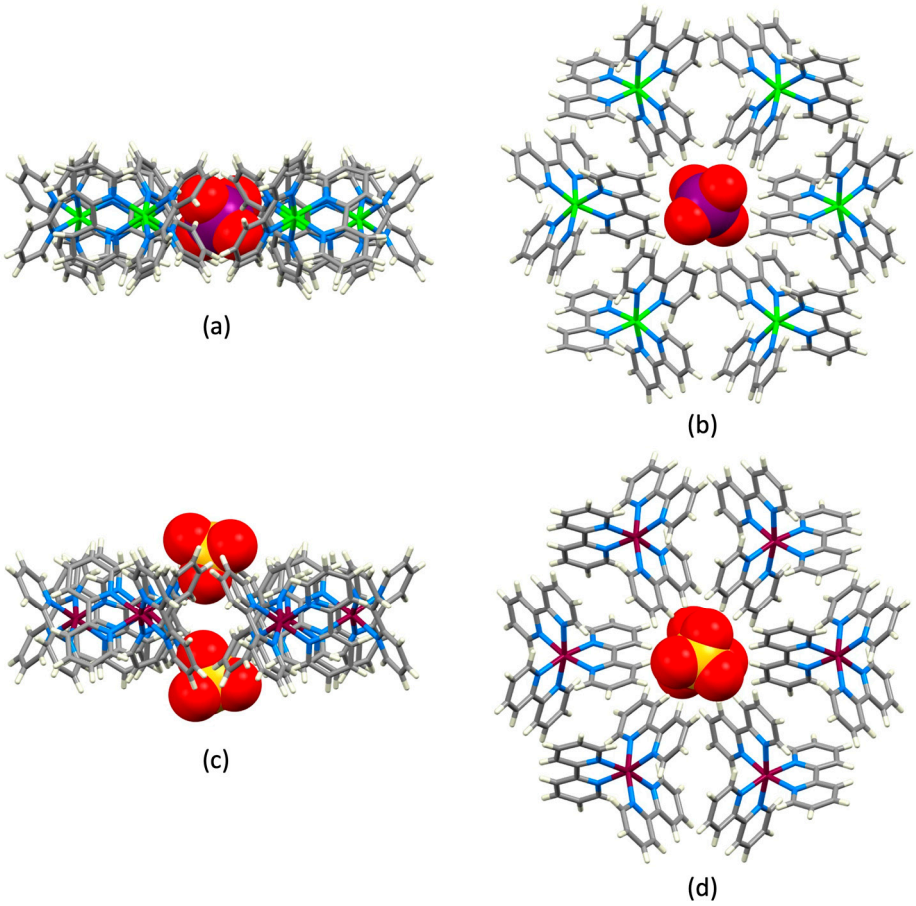

Figure 8. Structure Types I and II for $[XY_4]^{2-}$ containing compounds: (**a**,**b**) Structure Type I with the motif found in $[Zn(bpy)_3][CrO_4]_{0.5}[NO_3]\cdot 6.5H_2O$ (refcode XUJDEL) [29], and (**c**,**d**) structure Type II illustrated with the motif in $[Cu(bpy)_3][SO_4]\cdot 7.5H_2O$ (refcode ROLLOU) [56].

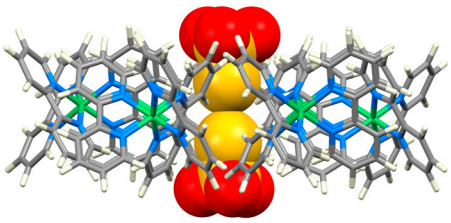

Figure 9. Arrangement of the thiosulfate ions within a $\{[Ni(bpy)_3]\}_6$-motif in $[Ni(bpy)_3][SSO_3]\cdot 7H_2O$ (refcode KOLXOY) [62].

Table 3. Structure Type I and II complexes with $[XY_4]^{m-}$ anions.

REFCODE Space Group	X Y	Structure Type	Range H…Y/Å (Mean H…Y/Å)	Range C…Y/Å (Mean C…Y/Å)	Range ∠C–H…Y/° (Mean ∠C–H…Y/°)	Range C…X/Å (Mean C…X/Å)	Refs.
XUJDEL *Ccc*2	Cr O	I	2.097–2.673 (2.347)	3.153–3.675 (3.373)	142.6–177.9 (160.1)	4.106–4.737 (4.339)	[29]
ELIHUY *C*2/*c*	Cr O	I	2.087–2.671 (2.319)	3.160–3.567 (3.354)	139.2–173.3 (161.4)	4.080–4.723 (4.333)	[28]
ROLLOU *C*2/*c*	S O	II	2.290–2.722 (2.566)	3.170–3.780 (3.464)	127.6–163.8 (141.0)	3.965–4.400 (4.227)	[56]
MOSHUZ *C*2/*c*	S O	II	2.287–2.786 (2.540)	3.087–3.701 (3.388)	116.2–158.5 (135.9)	3.860–4.430 (4.189)	[57]
KOKDUM	S	II	2.323–2.736	3.082–3.679	115.9–157.9	3.791–4.421	[58]

*C*2/*c*	O		(2.539)	(3.371)	(134.4)	(4.146)	
BPYNIS [a]	S	II	2.261–2.658	3.106–3.716	125.8–163.8	3.896–4.385	[59]
*C*2/*c*	O		(2.518)	(3.407)	(140.2)	(4.189)	
OREHEZ	S	II	2.308–2.769	3.090–3.696	116.3–157.3	3.816–4.416	[60]
*C*2/*c*	O		(2.551)	(3.388)	(134.8)	(4.157)	
LIFDOV	S	II	2.300–2.741	3.160–3.633	124.8–163.9	3.965–4.397	[61]
*C*2/*c*	O		(2.554)	(3.445)	(140.6)	(4.217)	
KOLXOY	S	II	Y = S 2.814–2.999 (2.901) Y = O 2.299–2.763 (2.556)	Y = S 3.735–3.895 (3.821) Y = O 3.187–3.756 (3.490)	Y = S 131.1–156.1 (143.5) Y = O 124.4–166.2 (145.4)	4.113–4.595 (4.323)	[62]
*C*2/*c*	O/S						
ROKHII	S	II	Y = S 2.774–3.010 (2.891) Y = O 2.320–2.785 (2.563)	Y = S 3.711–3.866 (3.798) Y = O 3.161–3.850 (3.502)	Y = S 127.7–155.7 (142.3) Y = O 124.3–167.4 (146.1)	4.090–4.637 (4.319)	[63]
*C*2/*c*	O/S						
RUYYIU [b]	Cr	II	2.257–2.778	3.185–3.685	113.9–169.9	4.016–4.697	[64]
*C*2/*c*	O		(2.576)	(3.381)	(132.7)	(4.313)	
NEMPAW [b]	Cr	II	2.198–2.816	3.197–3.779	115.0–172.1	4.078–4.700	[65]
*C*2/*c*	O		(2.602)	(3.408)	(133.1)	(4.333)	
VADPUM [b]	Cr	II	2.147–2.789	3.203–3.732	116.8–166.1	4.034–4.691	[66]
*C*2/*c*	O		(2.587)	(3.394)	(133.0)	(4.327)	
ELIMUH [a]	Mo	II	2.297–2.804	3.120–3.882	110.4–170.3	3.982–5.100	[67]
*C*2/*c*	O		(2.588)	(3.419)	(135.6)	(4.350)	

[a] H atom coordinates were not available in the CSD and were added in Mercury (see Section 2). [b] Disordered anion with common Cr position; all O sites were used in the analysis.

The compound (Λ)-[Mn(bpy)$_3$][ClO$_4$]$_2$·0.5C$_6$H$_4$-1,2-(COOEt)$_2$·0.5H$_2$O (refcode RAHRUO) [69] crystallizes in one of the Sohncke Space Groups [70], and (Λ)-[Mn(bpy)$_3$]$^{2+}$ cations assemble into sheets containing hexagonal motifs, not commented upon by the original authors [69]. In contrast to the crystal structures described earlier, this structure contains only (Λ)-sheets, and adjacent sheets are separated by a hydrogen-bonded network of water and diethyl phthalate molecules, as well as half of the perchlorate ions. The other half of the [ClO$_4$]$^-$ ions are accommodated within {[Mn^{II}(bpy)$_3$]}$_6$ motifs in a Type II arrangement. Each [ClO$_4$]$^-$ interacts with seven H3/H3′ atoms as well as four H4 atoms from six bpy ligands, and the metrics for the contacts are given in Table 4. The enantiomerically pure compounds (Λ)-[Zn(bpy)$_3$][ClO$_4$]$_2$·H$_2$O (refcode YUMJIZ) and (Λ)-[Ru(bpy)$_3$][ClO$_4$]$_2$·H$_2$O (refcode YUMJOF) are isomorphous, crystallizing in the Sohncke *C*2 space group [71]. The two independent (Λ)-[M(bpy)$_3$]$^{2+}$ cations form two crystallographically independent 2D-sheets that alternate through the lattice. The first comprises hexagonal {[M(bpy)$_3$]}$_6$ motifs and is a Type II structure with [ClO$_4$]$^-$ ions in pockets in the upper and lower surfaces of each sheet. Short CH$_{bpy}$...O contacts involving H3 and H4 are detailed in Table 4. In the Type II structural motif, the metal atoms of the [M(bpy)$_3$]$^{2+}$ cations are coplanar (or closely so). This is illustrated for (Λ)-[Zn(bpy)$_3$][ClO$_4$]$_2$·H$_2$O in Figure 10a. In the second independent sheet in (Λ)-[Zn(bpy)$_3$][ClO$_4$]$_2$·H$_2$O and (Λ)-[Ru(bpy)$_3$][ClO$_4$]$_2$·H$_2$O, the M atoms are not coplanar (Figure 10b), and disordered [ClO$_4$]$^-$ ions occupy partial occupancy sites above and below the sheet with extensive CH$_{bpy}$...O contacts.

Table 4. Structure Type II motifs with $[ClO_4]^-$ anions.

REFCODE Space Group	X Y	Structure Type	Range H…Y/Å (Mean H…Y/Å)	Range C…Y/Å (Mean C…Y/Å)	Range ∠C–H…Y/° (Mean ∠C–H…Y/°)	Range C…X/Å (Mean C…X/Å)	Refs.
RAHRUO [a] $C222_1$	Cl O	II	2.010–2.805 (2.569)	2.979–3.750 (3.419)	107.5–169.8 (137.8)	3.870–4.878 (4.369)	[69]
YUMJIZ [a] $C2$	Cl O	II	2.12–2.79 (2.52)	3.04–3.66 (3.31)	111.8–150.4 (130.1)	4.07–4.55 (4.27)	[71]
YUMJOF [a] $C2$	Cl O	II	2.19–2.82 (2.53)	3.07–3.61 (3.32)	107.0–148.4 (130.4)	4.05–4.64 (4.26)	[71]

[a] Disordered anion; all O sites used in the analysis.

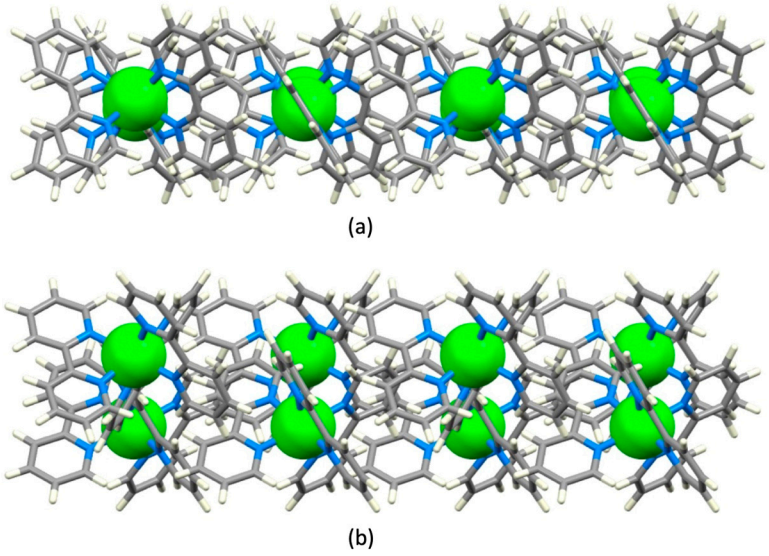

Figure 10. (**a**) Type II sheet of (Λ)-$[Zn(bpy)_3]^{2+}$ cations in (Λ)-$[Zn(bpy)_3][ClO_4]_2{\cdot}H_2O$ emphasizing the near coplanarity of the Zn(II) centers. (**b**) The second independent sheet of (Λ)-$[Zn(bpy)_3]^{2+}$ cations which has a 'ruffled' profile (CSD refcode YUMJIZ [71]). Both sheets are viewed along the crystallographic *b*-axis and perchlorate ions and water molecules are omitted.

Krausz et al. [71] have noted that the crystal packing in (Λ)-$[Zn(bpy)_3][ClO_4]_2{\cdot}H_2O$ and (Λ)-$[Ru(bpy)_3][ClO_4]_2{\cdot}H_2O$ is "nowhere near as efficient" as in *rac*-$[Zn(bpy)_3][ClO_4]_2$ and *rac*-$[Ru(bpy)_3][ClO_4]_2$. These two compounds (refcodes HEGMIP/01/02 [71–73] and ZAMGAV/01/02 [71,74,75]), along with $[Co(bpy)_3][ClO_4]_2$ (refcode MEFCEG [76]), $[Fe(bpy)_3][ClO_4]_2$ (refcode WOBTIQ [77]), and $[Ni(bpy)_3][ClO_4]_2$ (refcodes WADBOT/01/02 [78–80]) possess the same 2D-sheet structure with ordered perchlorate ions (Figure 11a). Note that in *rac*-$[Zn(bpy)_3][ClO_4]_2$ with refcode ZAMGAV01, about 8% of the metal sites are occupied by Ru [74]. Each sheet is homochiral, and alternating sheets contain (Λ)- or (Δ)-$[M(bpy)_3]^{2+}$ ions. Within a single sheet, $[M(bpy)_3]^{2+}$ cations form centered, hexagonal motifs as displayed in Figure 11b, and we label this motif a Type IV structure. Unlike the Type I, II and III structure types, each $[ClO_4]^-$ ion in the Type IV motif is not fully embraced by $[M(bpy)_3]^{2+}$ cations within a single sheet, but rather has short contacts to three cations in one sheet and three cations in an adjacent sheet; these involve H3, H4, H5 and H6 atoms of the bpy ligands and metric parameters for the $C–H_{bpy}...O_{perchlorate}$ interactions are given in Table 5. A comparison of these data confirms the similarity of the structures of this series of anhydrous $[M(bpy)_3][ClO_4]_2$ salts.

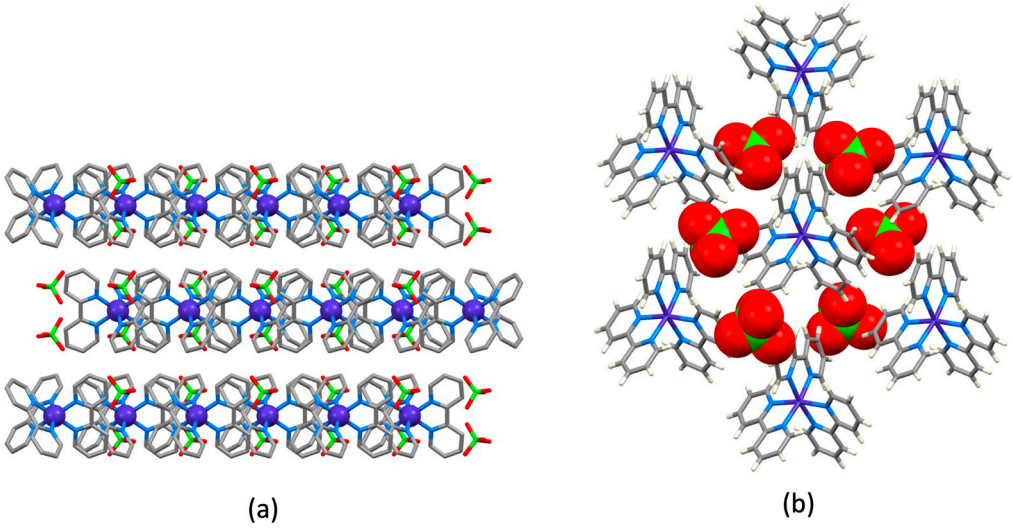

Figure 11. The structure of $[Co(bpy)_3][ClO_4]_2$ (refcode MEFCEG [76]). (**a**) Parts of three adjacent sheets viewed down the crystallographic *a*-axis; H atoms are omitted for clarity. (**b**) Part of one sheet viewed down the *c*-axis with anions in space-filling representation.

Table 5. Structure Type IV motifs with $[ClO_4]^-$ anions.

REFCODE Space Group	X Y	Structure Type	Range H…Y/Å (Mean H…Y/Å)	Range C…Y/Å (Mean C…Y/Å)	Range ∠C–H…Y/° (Mean ∠C–H…Y/°)	Range C…X/Å (Mean C…X/Å)	Refs.
MEFCEG *C*2/*c*	Cl O	IV	2.575–2.779 (2.688)	3.226–3.716 (3.419)	110.8–146.5 (125.2)	3.801–4.717 (4.304)	[76]
WADBOT *C*2/*c*	Cl O	IV	2.534–2.807 (2.692)	3.200–3.713 (3.417)	114.0–147.5 (124.7)	3.810–4.672 (4.279)	[78]
WADBOT01 *C*2/*c*	Cl O	IV	2.513–2.808 (2.694)	3.182–3.682 (3.409)	109.4–147.3 (123.8)	3.796–4.666 (4.252)	[79]
WADBOT02 *C*2/*c*	Cl O	IV	2.512–2.754 (2.625)	3.150–3.595 (3.335)	109.0–147.4 (123.3)	3.677–4.578 (4.183)	[80]
HEGMIP *C*2/*c*	Cl O	IV	2.411–2.794 (2.698)	3.151–3.706 (3.417)	105.9–151.1 (124.6)	3.873–4.668 (4.279)	[72]
HEGMIP01 *C*2/*c*	Cl O	IV	2.466–2.754 (2.688)	3.141–3.691 (3.409)	109.5–150.3 (124.6)	3.873–4.664 (4.273)	[71]
HEGMIP02 *C*2/*c*	Cl O	IV	2.526–2.726 (2.642)	3.140–3.698 (3.369)	109.1–147.8 (124.9)	3.732–4.565 (4.148)	[73]
ZAMGAV *C*2/*c*	Cl O	IV	2.522–2.790 (2.693)	3.216–3.521 (3.390)	107.4–145.6 (123.9)	3.776–4.593 (4.201)	[75]
ZAMGAV01 [a] *C*2/*c*	Cl O	IV	2.541–2.738 (2.642)	3.183–3.680 (3.372)	110.0–147.3 (125.1)	3.760–4.695 (4.263)	[74]
ZAMGAV02 *C*2/*c*	Cl O	IV	2.581–2.774 (2.675)	3.213–3.712 (3.405)	111.2–145.1 (125.1)	3.746–4.737 (4.285)	[71]
WOBTIQ *C*2/*c*	Cl O	IV	2.507–2.812 (2.664)	3.084–3.603 (3.366)	107.4–149.5 (122.8)	3.749–4.541 (4.207)	[77]

[a] H atom coordinates were not available in the CSD and were added in Mercury (see Section 2).

The final group of salts containing $[M(bpy)_3]^{q+}$ cations and $[XY_4]^{m-}$ ions features $[MCl_4]^{2-}$ (M = Fe, Zn, Cd, Pd) and $[MBr_4]^{2-}$ (M = Mn, Fe) ions. Of the eight salts in this group, five exhibit Type I or II structures. The $[PdCl_4]^{2-}$ salt is unique in the series because it contains a square-planar $[XY_4]^{m-}$ ion, and $[Ru(bpy)_3]_2[PdCl_4][Pd(ox)_2]\cdot 11H_2O$ (refcode TEXDAC) [81] has a Type I structure. The $[PdCl_4]^{2-}$ ions are embedded within homochiral sheets of (Λ)- or (Δ)-$[Ru(bpy)_3]^{2+}$ cations (Figure 12a), and the 2D-sheets are separated by hydrogen-bonded layers comprising $[Pd(ox)_2]^{2-}$ ions and water molecules. A comparison of Figure 12b with Figures 3b and 8b shows the similarity of the hexagonal motifs in the

Type I structures. In $[Ru(bpy)_3]_2[PdCl_4][Pd(ox)_2]\cdot 11H_2O$, the CH...Cl contacts primarily involve H3 and H3′ atoms with additional contacts to H4. Contact distances and angles are summarized in Table 6.

Table 6. Metrics for Type I and II motifs in salts containing $[MCl_4]^{2-}$ anions.

REFCODE Space Group	X Y	Structure Type	Range H…Y/Å (Mean H…Y/Å)	Range C…Y/Å (Mean C…Y/Å)	Range ∠C–H…Y/° (Mean ∠C–H…Y/°)	Range C…X/Å (Mean C…X/Å)	Refs.
TEXDAC $P2_1$	Pd Cl	I	2.582–3.030 (2.809)	3.460–3.980 (3.642)	117.6–176.5 (147.6)	3.762–5.770 (4.733)	[81]
BINZON $R\bar{3}c$	Cd Cl	II	2.609–3.037 (2.827)	3.490–3.856 (3.713)	127.0–156.2 (141.9)	4.41–5.04 (4.65)	[82]
XEQCUR [a] $R\bar{3}c$	Zn Cl	II	2.588–2.841 [b] (2.715)	3.508–3.861 (3.685)	141.6–155.8 (148.7)	4.390–4.458 (4.424)	[83]
NALSUQ $R\bar{3}c$	Fe Cl	II	2.551–2.816 (2.683)	3.472–3.840 (3.656)	141.7–156.6 (149.1)	4.387–4.455 (4.421)	[84]
SABGOV $P6_322$	Mn Br	II	2.863–2.979 (2.950)	3.802–4.012 (3.887)	136.3–158.6 (146.0)	4.335–4.730 (4.483)	[85]

[a] H atom coordinates were not available in the CSD and were added in Mercury (see Section 2). [b] There are also three contact distances of 3.090 Å, which are longer than the sum of the van der Waals radii + 0.1 Å (3.05 Å) which are analogous to the 3.037 Å contacts in BINZON.

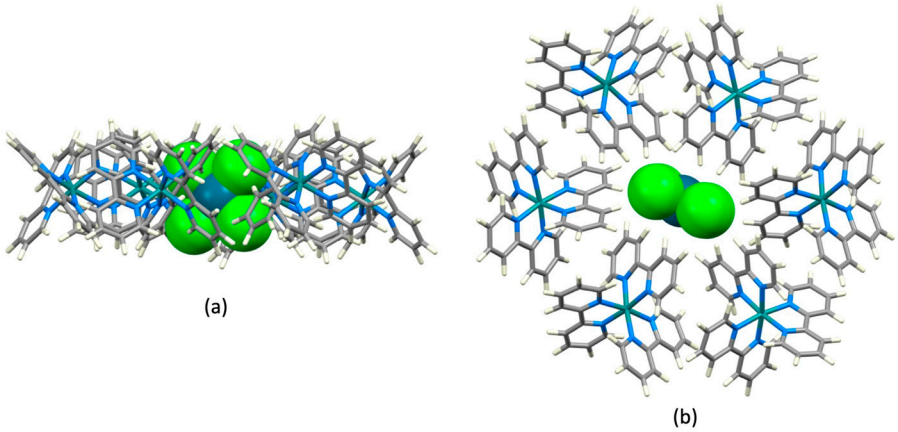

Figure 12. Structure Type I motif in $[Ru(bpy)_3]_2[PdCl_4][Pd(ox)_2]\cdot 11H_2O$ (CSD refcode TEXDAC) [81]. (**a**) One hexagonal motif within one sheet viewed down the crystallographic *b*-axis, and (**b**) the same unit viewed from above showing the bpy H3 and H3′ atoms directed towards the $[PdCl_4]^{2-}$ ion.

The packing in $[Ni(bpy)_3][CdCl_4]$ (refcode BINZON) [82], $[Ni(bpy)_3][ZnCl_4]$ (refcode XEQCUR) [83] and $[Fe(bpy)_3][FeCl_4]$ (refcode NALSUQ) [84] is reminiscent of that in $[Zn(bpy)_3][SSO_3]\cdot 7H_2O$ [63] and $[Ni(bpy)_3][SSO_3]\cdot 7H_2O$ [62] with a Type II motif (compare Figure 13a with Figure 9). Each $[CdCl_4]^{2-}$ exhibits short contacts to H3 and H4 atoms. $[Ni(bpy)_3][CdCl_4]$, $[Ni(bpy)_3][ZnCl_4]$ and $[Fe(bpy)_3][FeCl_4]$ crystallize in the trigonal space group $R\bar{3}c$ and each hexagonal motif, therefore, has 3-fold symmetry (Figure 13b). Distance and angle parameters for the embraces are given in Table 6. In contrast, $[M(bpy)_3][SSO_3]\cdot 7H_2O$ (M = Ni, Zn), $[Ni(bpy)_3][CdCl_4]$, $[Ni(bpy)_3][ZnCl_4]$ and $[Fe(bpy)_3][FeCl_4]$ are anhydrous and there are no hydrogen-bonded layers interleaved between the sheets of $[M(bpy)_3]^{2+}$ cations. The mixed oxidation state compound $[Co^{I}(bpy)_3]_3[Co^{II}(bpy)_3][MnBr_4]_2Br\cdot 2DMF$ (refcode SABGOV, DMF = *N*,*N*-dimethylformamide) crystallizes in the hexagonal Sohncke space group $P6_322$ [85]. The structure contains three independent Co atoms, and the Co(I) and Co(II) centers are distinguished by the Co–N bond lengths (average 2.095(2) Å for Co(I) and 2.124 Å for Co(II)). Although the packing was not described in detail in the original publication [85], we can use the reported Co–N bond length data to describe the structure in terms of alternating homochiral

sheets containing (i) (Δ)-[Co^{I}(bpy)$_3$]$^+$ and [MnBr$_4$]$^{2-}$ ions (lower sheet in Figure 14a) and (ii) (Λ)-[Co^{I}(bpy)$_3$]$^+$, (Λ)-[Co^{II}(bpy)$_3$]$^+$ and Br$^-$ ions (upper sheet in Figure 14a). The DMF solvent molecules were disordered, and detailed positions are not available. The 2D-sheet containing (Δ)-[Co^{I}(bpy)$_3$]$^+$ and [MnBr$_4$]$^{2-}$ ions adopts a Type II structure (Figure 14b and Table 6) while the Br$^-$ ion is at the center of a {Co(bpy)$_3$}$_6$-motif (a Type I structure [20]).

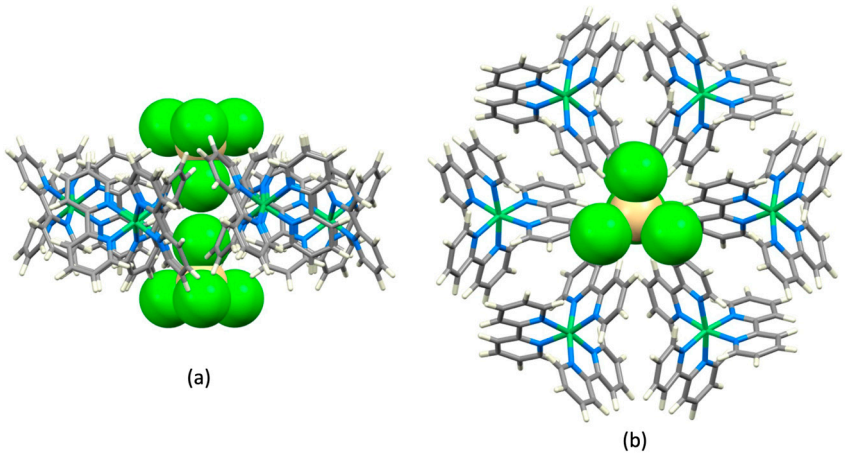

Figure 13. Structure Type II motif in [Ni(bpy)$_3$][CdCl$_4$] (refcode BINZON) [82] viewed (**a**) from the side and (**b**) from above.

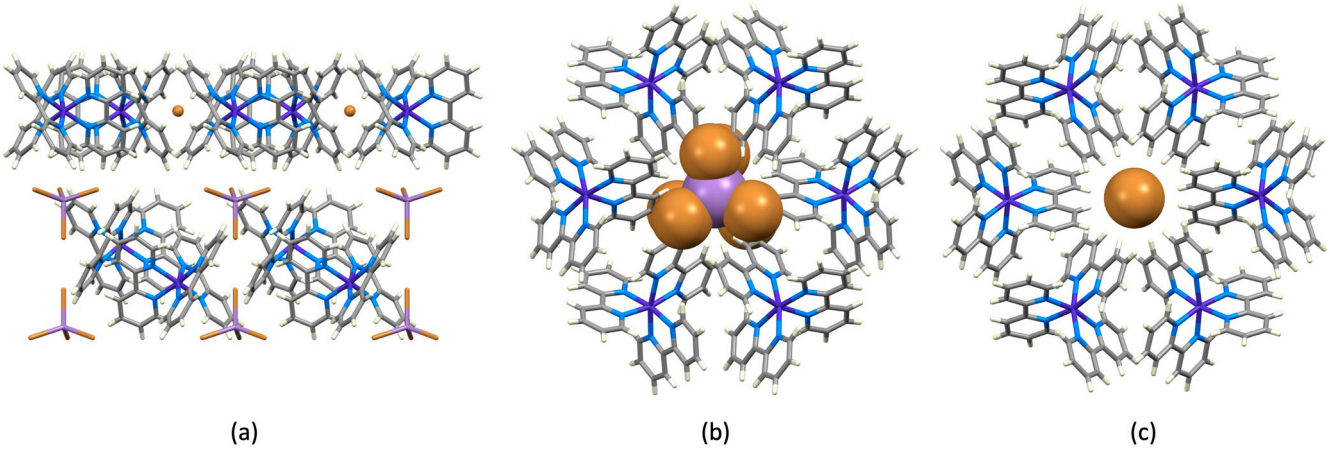

Figure 14. The structure of [Co^{I}(bpy)$_3$]$_3$[Co^{II}(bpy)$_3$][MnBr$_4$]$_2$Br·2DMF (refcode SABGOV [85]). (**a**) Parts of adjacent homochiral 2D-sheets viewed down the crystallographic *a*-axis; the Br$^-$ ions in the top layer are shown in ball-and-stick representation for clarity. All [MnBr$_4$]$^{2-}$-containing sheets have (Δ)-[Co^{I}(bpy)$_3$]$^+$ ions and all Br$^-$-containing sheets include equal numbers of (Λ)-[Co^{I}(bpy)$_3$]$^+$ and (Λ)-[Co^{II}(bpy)$_3$]$^+$ ions. (**b**) The Type II motif from the lower layer in diagram (**a**) viewed down the *c*-axis. (**c**) The Type I motif from the upper layer in diagram (**a**) viewed down the *c*-axis.

The crystal structure of [Fe(bpy)$_3$][FeCl$_4$]$_2$ (refcode HUMGEB) [86] comprises heterochiral sheets of [M(bpy)$_3$]$^{2+}$ cations and this precludes the appearance of the hexagonal motifs, and neither of the remaining two compounds in the tetrahalidometallate series (refcodes YAVCIL and PABRUJ) exhibits a homochiral layer structure. Thus, of the eight tetrahalidometallate salts, five exhibit Type I and II anion embraces, representing 62.5% of this set of structures.

7. Conclusions

We have used Conquest (version 2022.3.0) [23] to search the CSD [21] for the $[M(bpy)_3]$ motif (M = any transition metal) combined with XY_3, XY_4 or XY_5 units in which X and Y are any atom; no structures containing $[XY_5]^{m-}$ anions were found. After reducing the structures to those with $[XY_3]^{m-}$ and $[XY_4]^{m-}$ anions, two sets, respectively, of 12 and 50 structures, remained for detailed analysis.

Of the 12 structures which contain $[XY_3]^{m-}$ anions, all are layer assemblies and all but one possess homochiral sheets containing (Λ)- or (Δ)-$[M(bpy)_3]^{q+}$ cations in hexagonal motifs. The doubly charged sulfite ion is accommodated in the center of the motif (Type I structure, Table 1) while singly-charged nitrate ions tend to reside in pockets in the top and bottom surfaces of each sheet (Types II and III, Tables 1 and 2). However, when strong hydrogen bond donors or acceptors, such as the hydrogen phthalate ion, are introduced into the assembly, a preference for the nitrate ion to be involved in a hydrogen-bonded network is observed.

The 50 structures with $[XY_4]^{m-}$ anions fall into four groups. The first group comprises $[SO_4]^{2-}$, $[SSO_3]^{2-}$, $[CrO_4]^{2-}$, and $[MoO_4]^{2-}$ salts, and all exhibit homochiral sheet structures with hexagonal $\{M(bpy)_3\}_6$ motifs embracing the tetrahedral anions in either a Type I or II structure (Table 3). In the second group comprising 25 perchlorate salts, three structures exhibit the Type II motif (Table 4), while five exhibit a centered hexagonal motif (Type IV, Table 5). Most salts containing $[ClO_4]^-$ do not conform to the patterns established for the $[SO_4]^{2-}$, $[SSO_3]^{2-}$, $[CrO_4]^{2-}$, and $[MoO_4]^{2-}$ salts. Similarly, homochiral layers are not found in any of the three $[BF_4]^-$ salts (the third group of structures). The fourth group contains eight tetrahalidometallate salts, and 62.5% of these exhibit Type I and II anion embraces.

The identification of a series of related and ubiquitous motifs in the solid-state structures of $[M(bpy)_3]^{q+}$ salts provides a new and alternative approach to considering their crystal supramolecular chemistry. The results of our analysis complement the discussion by Breu et al. regarding packing interactions in $[Cr(bpy)_3]^{n+}[PF_6]_n$ (n = 0–3) [87].

Author Contributions: The authors contributed equally to the writing of this work. Conceptualization, E.C.C.; data mining and evaluation, E.C.C. and C.E.H. All authors have read and agreed to the published version of the manuscript.

Funding: This research received no external funding.

Data Availability Statement: Not applicable.

Acknowledgments: We thank the University of Basel for support.

Conflicts of Interest: The authors declare no conflict of interest.

References

1. Blau, F. Die Destillation pyridinmonocarbonsaurer Salze. *Ber. Dtsch. Chem. Ges*. **1888**, *21*, 1077–1078. https://doi.org/10.1002/cber.188802101201.
2. Constable, E.C.; Housecroft, C.E. The Early Years of 2,2′-Bipyridine—A Ligand in Its Own Lifetime. *Molecules* **2019**, *24*, 3951. https://doi.org/10.3390/molecules24213951.
3. Kaes, C.; Katz, A.; Hosseini, M.W. Bipyridine: The Most Widely Used Ligand. A Review of Molecules Comprising at Least Two 2,2′-Bipyridine Units. *Chem. Rev*. **2000**, *100*, 3553–3590. https://doi.org/10.1021/cr990376z.
4. Summers, L.A. The Bipyridines. *Adv. Heterocycl. Chem.* **1984**, *35*, 281–374. https://doi.org/10.1016/S0065-2725(08)60151-8.
5. Constable, E.C. Homoleptic Complexes of 2,2′-Bipyridine. *Adv. Inorg. Chem.* **1989**, *34*, 1–63. https://doi.org/10.1016/S0898-8838(08)60014-8.
6. Lindoy, L.F.; Livingstone, S.E. Complexes of iron(II), cobalt(II) and nickel(II) with α-diimines and related bidentate ligands. *Coord. Chem. Rev.* **1967**, *2*, 173–193. https://doi.org/10.1016/S0010-8545(00)80204-0.
7. McWhinnie, W.R.; Miller, J.D. The Chemistry of Complexes Containing 2,2′-Bipyridyl, 1,10-Phenanthroline, or 2,2′,6′,2″-Terpyridyl as Ligands. *Adv. Inorg. Chem. Radiochem.* **1970**, *12*, 135–215. https://doi.org/10.1016/S0065-2792(08)60049-7.
8. Brandt, W.W.; Dwyer, F.P.; Gyarfas, E.D. Chelate Complexes of 1,10-Phenanthroline and Related Compounds. *Chem. Rev.* **1954**, *54*, 959–1017. https://doi.org/10.1021/cr60172a003.
9. Smith, A.P.; Fraser, C.L. Bipyridine Ligands. In *Comprehensive Coordination Chemistry*, 2nd ed.; McCleverty, J.A., Meyer, T.J., Eds.; Elsevier: Oxford, UK, 2003; pp. 1–23. https://doi.org/10.1016/B0-08-043748-6/01103-8.

10. Grice, K.A.; Nganga, J.K.; Naing, M.D.; Angeles-Boza, A.M. Bipyridine Ligands. In *Comprehensive Coordination Chemistry*, 3rd ed.; Constable, E.C., Parkin, G., Que, L., Eds.; Elsevier: Oxford, UK, 2021; pp. 60–77. https://doi.org/10.1016/B978-0-08-102688-5.00067-2.
11. Schilt, A.A. Analytical Applications of 1,10-Phenanthroline and Related Compounds. In *International Series of Monographs on Analytical Chemistry*; Pergamon: Oxford, UK, 1969; Volume 32, pp. 10–53. https://doi.org/10.1016/B978-0-08-012877-1.50005-0.
12. McKenzie, E.D. The steric effect in bis(2,2′-bipyridyl) and bis(1,10-phenanthroline) metal compounds. *Coord. Chem. Rev.* **1971**, *6*, 187–216. https://doi.org/10.1016/S0010-8545(00)80039-9.
13. Constable, E.C. Forty years on—Covalent hydration of transition metal complexes revisited. *Polyhedron* **2016**, *103B*, 295–306. https://doi.org/10.1016/j.poly.2015.03.016.
14. Constable, E.C.; Housecroft, C.E. More hydra than Janus—Non-classical coordination modes in complexes of oligopyridine ligands. *Coord. Chem. Rev.* **2017**, *350*, 84–104. https://doi.org/10.1016/j.ccr.2017.06.006.
15. Constable, E.C.; Housecroft, C.E. 'Simple' Oligopyridine Complexes—Sources of Unexpected Structural Diversity. *Aust. J. Chem.* **2020**, *73*, 390–398. https://doi.org/10.1071/CH19621.
16. Dance, I.; Scudder, M. Supramolecular motifs: Sextuple aryl embraces in crystalline [M(2,2′-bipy)$_3$] and related complexes. *J. Chem. Soc. Dalton Trans*. **1998**, 1341–1350. https://doi.org/10.1039/A707237F.
17. Dance, I. Intermolecular Embraces and Intermolecular Energies. *Mol. Cryst. Liq. Cryst.* **2006**, *440*, 265–293. https://doi.org/10.1080/15421400590958593.
18. Dance, I. Inorganic intermolecular motifs, and their energies. *CrystEngComm* **2003**, *5*, 208–221. https://doi.org/10.1039/B304667M.
19. Dance, I. Distance criteria for crystal packing analysis of supramolecular motifs. *New J. Chem.* **2003**, *27*, 22–27. https://doi.org/10.1039/B206867B.
20. Constable, E.C.; Housecroft, C.E. Halide Ion Embraces in Tris(2,2′-bipyridine)metal Complexes. *Crystals* **2020**, *10*, 671. https://doi.org/10.3390/cryst10080671.
21. Groom, C.R.; Bruno, I.J.; Lightfoot, M.P.; Ward, S.C. The Cambridge Structural Database. *Acta Cryst.* **2016**, *B72*, 171–179. https://doi.org/10.1107/S2052520616003954.
22. Ruiz-Pérez, C.; Lorenzo Luis, P.A.; Lloret, F.; Julve, M. Dimensionally controlled hydrogen-bonded nanostructures: Synthesis, structure, thermal and magnetic behaviour of the tris-(chelated)nickel(II) complex [Ni(bipy)$_3$Cl$_2$]·5.5H$_2$O (bipy = 2,2′-bipyridyl). *Inorg. Chim. Acta* **2002**, *336*, 131–136. https://doi.org/10.1016/S0020-1693(02)00840-X.
23. Bruno, I.J.; Cole, J.C.; Edgington, P.R.; Kessler, M.; Macrae, C.F.; McCabe, P.; Pearson, J.; Taylor, R. New software for searching the Cambridge Structural Database and visualising crystal structures. *Acta Cryst.* **2002**, *B58*, 389–397. https://doi.org/10.1107/S0108768102003324.
24. Macrae, C.F.; Sovago, I.; Cottrell, S.J.; Galek, P.T.A.; McCabe, P.; Pidcock, E.; Platings, M.; Shields, G.P.; Stevens, J.S.; Towler, M.; et al. Mercury 4.0: From visualization to analysis, design and prediction. *J. Appl. Cryst.* **2020**, *53*, 226–235. https://doi.org/10.1107/S1600576719014092.
25. Thuéry, P.; Harrowfield, J. Uranyl Ion Complexes with 1,1′-Biphenyl-2,2′,6,6′-tetracarboxylic Acid: Structural and Spectroscopic Studies of One- to Three-Dimensional Assemblies. *Inorg. Chem.* **2015**, *54*, 6296–6305. https://doi.org/10.1021/acs.inorgchem.5b00596.
26. Handke, M.; Wu, Y.; Li, Y.; Hu, C.T.; Ward, M.D. Encapsulation of the [Ru(bpy)$_3$]$^{2+}$ luminophore in a unique hydrogen-bonded host framework. *CrystEngComm* **2020**, *22*, 3749–3752. https://doi.org/10.1039/D0CE00680G.
27. Vasilchenko, D.; Topchiyan, P.; Baidina, I.; Korolkov, I.; Filatov, E.; Zvereva, V.; Plyusnin, P.; Slavinskaya, E.; Gerasimov, E. Double complex salts containing [Pt(NO3)6]2-anion and Rh(III) complex cations: Synthesis, structure and utilisation for preparing (Rh–Pt)/CeO$_2$ catalysts. *J. Mol. Struct.* **2020**, *1211*, 128108. https://doi.org/10.1016/j.molstruc.2020.128108.
28. Wojciechowska, A.; Staszak, Z.; Bronowska, W.; Pietraszko, A.; Cieślak-Golonka, M. Crystal structure and 4.2 K electronic spectrum of [Co(bpy)$_3$](CrO$_4$)$_{0.5}$NO$_3$·7H$_2$O, a double salt containing uncoordinated chromate ion. *J. Mol. Struct.* **2003**, *654*, 197–204. https://doi.org/10.1016/S0022-2860(03)00215-1.
29. Wojciechowska, A.; Bronowska, W.; Pietraszko, A.; Staszak, Z.; Cieślak-Golonka, M. Synthesis, crystal structure and spectroscopic characterisation of double salt [Zn(bpy)$_3$](CrO$_4$)$_{0.5}$NO$_3$6.5H$_2$O. *J. Mol. Struct.* **2002**, *608*, 151–160. https://doi.org/10.1016/S0022-2860(01)00924-3.
30. Jaeger, F.M.; van Dijk, J.A. On some complex dipyridyl-salts of nickel and copper. *J. Proc. K. Ned. Akad. Wet. B* **1935**, *38*, 972–977.
31. Henling, L.M.; Marsh, R.E. Some more space-group corrections. *Acta Crystallogr. Sect. C* **2014**, *70*, 834–836. https://doi.org/10.1107/S2053229614017549.
32. Zhuge, F.; Wu, B.; Liang, J.; Yang, J.; Liu, Y.; Jia, C.; Janiak, C.; Tang, N.; Yang, X.-J. Full- or Half-Encapsulation of Sulfate Anion by a Tris(3-pyridylurea) Receptor: Effect of the Secondary Coordination Sphere. *Inorg. Chem.* **2009**, *48*, 10249–10256. https://doi.org/10.1021/ic9012685.
33. Mustafina, A.R.; Skripacheva, V.V.; Gubaidullin, A.T.; Latipov, S.K.; Toropchina, A.V.; Yanilkin, V.V.; Solovieva, S.E.; Antipin, I.S.; Konovalov, A.I. Outer-Sphere Association of *p*-Sulfonatothiacalix[4]arene and Tetrasulfonatomethylated Calix[4]resorcinarene with Cobalt(III) Tris(dipyridyl): The Effect on the Spectral and Electrochemical Properties of the Latter. *Inorg. Chem.* **2005**, *44*, 4017–4023. https://doi.org/10.1021/ic050038i.
34. Yu, K.; Chen, W.-L.; Zhou, B.-B.; Li, Y.-G.; Yu, Y.; Su, Z.-H.; Gao, S.; Chen, Y. New extended poly(oxomolybdophosphates) based on strontium(II) linkers. *CrystEngComm* **2011**, *13*, 3417–3424. https://doi.org/10.1039/c0ce00727g.

35. Scott, R.T.W.; Parsons, S.; Murugesu, M.; Wernsdorfer, W.; Christou, G.; Brechin, E.K. Linking Centered Manganese Triangles into Larger Clusters: A {Mn_{32}} Truncated Cube. *Angew. Chem. Int. Ed.* **2005**, *44*, 6540–6543. https://doi.org/10.1002/anie.200501881.
36. Andres, R.; Brissard, M.; Gruselle, M.; Train, C.; Vaissermann, J.; Malezieux, B.; Jamet, J.P.; Verdaguer, M. Rational Design of Three-Dimensional (3D) Optically Active Molecule-Based Magnets: Synthesis, Structure, Optical and Magnetic Properties of {$[Ru(bpy)_3]^{2+}$, ClO_4^-, $[Mn^{II}Cr^{III}(ox)_3]^-\}_n$ and {$[Ru(bpy)_2ppy]^+$, $[M^{II}Cr^{III}(ox)_3]^-\}_n$, with M^{II} = Mn^{II}, Ni^{II}. X-ray Structure of {$[\Delta Ru(bpy)_3]^{2+}$, ClO_4^-, $[\Delta Mn^{II}\Delta Cr^{III}(ox)_3]^-\}_n$ and {$[\Lambda Ru(bpy)_2ppy]^+$, $[\Lambda Mn^{II}\Lambda Cr^{III}(ox)_3]^-\}_n$. *Inorg. Chem*. **2001**, *40*, 4633–4640. https://doi.org/10.1021/ic010363f.
37. Coronado, E.; Galán-Mascarós, J.R.; Gómez-García, C.J.; Martínez-Agudo, J.M. Molecule-Based Magnets Formed by Bimetallic Three-Dimensional Oxalate Networks and Chiral Tris(bipyridyl) Complex Cations. The Series $[Z^{II}(bpy)_3][ClO_4][M^{II}Cr^{III}(ox)_3]$ (Z^{II} = Ru, Fe, Co, and Ni; M^{II} = Mn, Fe, Co, Ni, Cu, and Zn; ox = Oxalate Dianion). *Inorg. Chem*. **2001**, *40*, 113–120. https://doi.org/10.1021/ic0008870.
38. Hernández-Molina, M.; Lloret, F.; Ruiz-Pérez, C.; Julve, M. Weak Ferromagnetism in Chiral 3-Dimensional Oxalato-Bridged Cobalt(II) Compounds. Crystal Structure of $[Co(bpy)_3][Co_2(ox)_3]ClO_4$. *Inorg. Chem*. **1998**, *37*, 4131–4135. https://doi.org/10.1021/ic980306v.
39. Decurtins, S.; Schmalle, H.W.; Pellaux, R.; Schneuwly, P.; Hauser, A. Chiral, Three-Dimensional Supramolecular Compounds: Homo- and Bimetallic Oxalate- and 1,2-Dithiooxalate-Bridged Networks. A Structural and Photophysical Study. *Inorg. Chem.* **1996**, *35*, 1451–1460. https://doi.org/10.1021/ic950791j.
40. Stebler, M.; Gutierrez, A.; Ludi, A.; Burgi, H.-B. Synthesis and crystal structure of tris(2,2′-bipyridine)rhenium(2+) perrhenate. *Inorg. Chem*. **1987**, *26*, 1449–1451. https://doi.org/10.1021/ic00256a025.
41. Fang, Y.; Jie, Q.; Huang, C. Synthesis and Crystal Structure of a Keggin-Polymolybdate Complex $\{PMo^{VI}_7Mo^{V}_4V^{V}O_{40}(V^{IV}O)_2[Co(bipy)_2(H_2O)]_2\}[Co(bipy)_3]_2\{PMo^{VI}_7Mo^{V}_4V^{V}O_{40}(V^{IV}O)_2\}\cdot 6H_2O$. *Beihua Daxue Xuebao Ziran Kexueban* **2010**, *11*, 213–217.
42. Jacobs, G.; Speeke, F. The unit cell and space group of the complex tridipyridyl-nickel sulfate. *Acta Cryst.* **1955**, *8*, 67–68. https://doi.org/10.1107/S0365110X55000261.
43. Constable, E.C.; Housecroft, C.E. When Stereochemistry Raised Its Ugly Head in Coordination Chemistry—An Appreciation of Howard Flack. *Chemistry* **2020**, *2*, 759–776. https://doi.org/10.3390/chemistry2030049.
44. McNaught, A.D.; Wilkinson, A. *Compendium of Chemical Terminology*, 2nd ed.; IUPAC Gold Book; Online Version (2019-) created by Chalk, S.J.; Blackwell Scientific Publications: Oxford, UK, 1997; ISBN 0-9678550-9-8.
45. Connelly, N.G.; Damhus, T.; Hartshorn, R.M.; Hutton, A.T. (Eds.) *Nomenclature of Inorganic Chemistry, IUPAC Recommendations 2005*; IUPAC Red Book; RSC Publishing: Cambridge, UK, 2005.
46. Luo, Q.; Chen, Y.-Q.; Peng, H.-Q.; Ji, Q.; Wang, X.-X.; Wei, L.; Zhong, Q.-Y.; Chen, W.-T. Preparation, characterization, and photoluminescent and semiconductive properties of an iron compound. *Inorg. Nano-Metal Chem*. **2022**. https://doi.org/10.1080/24701556.2021.2025094.
47. Lin, J.-M.; Chen, W.-B.; Lin, X.-M.; Lin, A.-H.; Ma, C.-Y.; Dong, W.; Tian, C.-E. Syntheses, structures and multi-photoluminescence images with confocal microscopy for three 5,5′-azotetrazolate (AZT) based Zn(II) and Ni(II) complexes. *Chem. Commun*. **2011**, *47*, 2402–2404. https://doi.org/10.1039/c0cc03720f.
48. Evstifeev, I.; Kiskin, M.; Eremenko, I. Tris(2,2′-bipyridine)-cobalt(ii) dinitrate acetonitrile solvate monohydrate. *CSD Commun.* **2012**. https://doi.org/10.5517/ccxyc5c.
49. Shen, L.; Han, Z.; Brennessel, W.W.; Holland, P.L.; Eisenberg, R. Tris(2,2′-bipyridine)-nickel(ii) dinitrate acetonitrile solvate monohydrate. *CSD Commun.* **2012**. https://doi.org/10.5517/ccz8thj.
50. Kumar, D.; Kapoor, I.P.S.; Singh, G.; Goel, N.; Singh, U.P. Preparation, X-ray crystallography and thermolysis of transition metal nitrates of 2,2′-bipyridine (Part 63). *J. Therm. Anal. Calorim*. **2012**, *107*, 325–334. https://doi.org/10.1007/s10973-011-1781-5.
51. Tomić, Z.; Prelesnik, B.; Karanović, L.; Poleti, D. Crystal structure of di-[tris(2,2′-bipyridine)nickel(II)] hydrogen phthalate trinitrate tetrahydrate. *J. Serb. Chem. Soc.* **1996**, *61*, 97–106.
52. Miao, X.-H.; Zhu, L.-G. Synthesis, supramolecular structures and catalytic properties of nickel(II) 3-sulfobenzoate complexes with chelating amine ligands. *CrystEngComm* **2009**, *11*, 2500–2509. https://doi.org/10.1039/b907453h.
53. Jurić, M.; Planinić, P.; Brničević, N.; Milić, D.; Matković-Čalogović, D.; Pajić, D.; Zadro, K. New Heterometallic (Cu^{II} and Cr^{III}) Complexes—First Crystal Structure of an Oxalate-Bridged Ferromagnetically Coupled $[Cu^{II}Cr^{III}Cu^{II}]$ System. *Eur. J. Inorg. Chem.* **2006**, *2006*, 2701–2710. https://doi.org/10.1002/ejic.200501092.
54. Jurić, M.; Planinić, P.; Žilić, D.; Rakvin, B.; Prugovečki, B.; Matković-Čalogović, D. A new heterometallic (Ni^{2+} and Cr^{3+}) complex—Crystal structure and spectroscopic characterization. *J. Mol. Struct*. **2009**, *924*, 73–80. https://doi.org/10.1016/j.molstruc.2008.10.052.
55. Muzioł, T.M.; Tereba, N.; Podgajny, R.; Kędziera, D.; Wrzeszcz, G. Solvent-assisted structural conversion involving bimetallic complexes based on the tris(oxalato) ferrate(III) unit with the green → blue → red crystal color sequence. *Dalton Trans.* **2019**, *48*, 11536–11546. https://doi.org/10.1039/c9dt02216c.
56. Xu, F.; You, W.; Huang, W. Tris(2,2′-bipyridyl-κ^2N,N')copper(II) sulfate 7.5-hydrate. *Acta Crystallogr. Sect. E* **2009**, *65*, m129–m130. https://doi.org/10.1107/S1600536808043821.

57. Avdeeva, V.V.; Vologzhanina, A.V.; Goeva, L.V.; Malinina, E.A.; Kuznetsov, N.T. Boron Cluster Anions $[B_nH_n]^{2-}$ (n = 10, 12) in Reactions of Iron(II) and Iron(III) Complexation with 2,2′-Bipyridyl and 1, 10-Phenanthroline. *Z. Anorg. Allg. Chem.* **2014**, *640*, 2149–2160. https://doi.org/10.1002/zaac.201400137.
58. Li, Y.-L.; Yang, Y.-Q.; Mao, F.-F.; Chen, Z.-M. Synthesis, Crystal Structure, and Fluorescent and Thermal Stability Properties of Two New Cobalt(II) Complexes with 2,2′-Bipy as Ligand. *Chin. J. Struct. Chem.* **2019**, *38*, 769–776. https://doi.org/10.14102/j.cnki.0254-5861.2011-2117.
59. Wada, A.; Sakabe, N.; Tanaka, J. The crystal structure of tris(2,2′-bipyridyl)nickel(II) sulphate hydrate, $[Ni(C_{10}H_8N_2)_3]SO_4{\cdot}7.5H_2O$. *Acta Crystallogr. Sect. B* **1976**, *32*, 1121–1127. https://doi.org/10.1107/S0567740876004809.
60. Eom, G.H.; Park, H.M.; Hyun, M.Y.; Jang, S.P.; Kim, C.; Lee, J.H.; Lee, S.J.; Kim, S.-J.; Kim, Y. Anion effects on the crystal structures of Zn^{II} complexes containing 2,2′-bipyridine: Their photoluminescence and catalytic activities. *Polyhedron* **2011**, *30*, 1555–1564. https://doi.org/10.1016/j.poly.2011.03.040.
61. Huang, Q.; Diao, L.; Zhang, C.; Lei, F. Cyclic Water Clusters in Tape-Like and Cage-Like Structures. *Molecules* **2011**, *16*, 2871–2883. https://doi.org/10.3390/molecules16042871.
62. Freire, E.; Baggio, S.; Mombru, A.; Baggio, R. Tris(2,2′-bipyridyl-*N,N*′)nickel(II) thiosulfate heptahydrate. *Acta Crystallogr. Sect. C* **2000**, *56*, 541–543. https://doi.org/10.1107/S0108270100001414.
63. Baggio, S.; Pardo, M.I.; Baggio, R.; Garland, M.T. Tris(2,2′-bipyridyl-*N,N*′)zinc(II) Thiosulfate Heptahydrate. *Acta Crystallogr. Sect. C* **1997**, *53*, 1570–1572. https://doi.org/10.1107/S0108270197008615.
64. Wojciechowska, A.; Pietraszko, A.; Bronowska, W.; Staszak, Z.; Jezierska, J.; Cieślak-Golonka, M. Geometric distortions of octahedral cations and tetrahedral anions in disordered $[Cu(bpy)_3]CrO_4{\cdot}7.5H_2O$ crystal—A comparative study. *Polyhedron* **2010**, *29*, 2574–2581. https://doi.org/10.1016/j.poly.2010.06.003.
65. Wojciechowska, A.; Staszak, Z.; Bronowska, W.; Pietraszko, A.; Cieślak-Golonka, M. Spectroscopic and structural studies of chromate ions in zinc complexes with 2,2′-bipyridine. Analysis of the lowest triplet states in the CrO_4^{2-} entity. *Polyhedron* **2001**, *20*, 2063–2072. https://doi.org/10.1016/S0277-5387(01)00806-3.
66. Pietraszko, A.; Bronowska, W.; Wojciechowska, A.; Staszak, Z.; Cieślak-Golonka, M. One-, Two- and Non-Coordinated CrO_4^{2-} Entity in the Nickel(II) Complexes. Structural and Spectroscopic Investigation. *Pol. J. Chem.* **2002**, *76*, 309–324.
67. Zeng, Q.-X.; Yang, G.-Y.; Xu, J.-Q. Hydrothermal synthesis and crystal structure of $[Ni(2,2'\text{-bpy})_3]MoO_4.7.5H_2O$. *Jiegou Huaxue* **2003**, *22*, 336–340.
68. Cheung, E.Y.; Fujii, K.; Guo, F.; Harris, K.D.M.; Hasebe, S.; Kuroda, R. Structural Chemistry of a New Chiral Anhydrous Phase of $Ru(bipy)_3(ClO_4)_2$ Established from Powder X-ray Diffraction Analysis. *Cryst. Growth Des.* **2011**, *11*, 3313–3317. https://doi.org/10.1021/cg200379h.
69. Fernández, G.; Corbella, M.; Alfonso, M.; Stoeckli-Evans, H.; Castro, I. A Comparative XAS and X-ray Diffraction Study of New Binuclear Mn(III) Complexes with Catalase Activity. Indirect Effect of the Counteranion on Magnetic Properties. *Inorg. Chem.* **2004**, *43*, 6684–6698. https://doi.org/10.1021/ic0348897.
70. Sohncke, L. *Entwickelung Einer Theorie der Krystallstruktur*; B.G. Teubner: Leipzig, Germany, 1879.
71. Krausz, E.; Riesen, H.; Rae, A.D. Crystal Structures of and Polarized Absorption-Spectroscopy in Racemic and Resolved $[Ru(bpy)_3](ClO_4)_2$ and $[Zn(bpy)_3](ClO_4)_2$ Bpy = 2,2′-Bipyridine. *Aust. J. Chem.* **1995**, *48*, 929–954. https://doi.org/10.1071/CH9950929.
72. Harrowfield, J.M.; Sobolev, A.N. The Crystal Structure of Tris(2,2′-bipyridine)ruthenium(II) Perchlorate. *Aust. J. Chem.* **1994**, *47*, 763–767. https://doi.org/10.1071/CH9940763.
73. Moore, C.; Grotjahn, D.; Rheingold, A. Tris(2,2′-Bipyridine)-ruthenium(ii) diperchlorate. *CSD Commun.* **2010**. https://doi.org/10.5517/ccvqzs9.
74. Klement, U.; Trumbach, D.; Yersin, H. Crystal structure of tris(2,2′-bipyridyl)-zinc(II) Perchlorate, $(Zn(C_{10}H_8N_2)_3)(ClO_4)_2$ *Z. Kristallogr.—Cryst. Mater.* **1995**, *210*, 228–228. https://doi.org/10.5517/cc3q00t.
75. Chen, X.-M.; Wang, R.-Q.; Yu, X.-L. Tris(2,2′-bipyridine)zinc(II) Perchlorate. *Acta Crystallogr. Sect. C* **1995**, *51*, 1545–1547. https://doi.org/10.1107/S0108270195000321.
76. Yao, J.-C.; Ma, L.-F.; Yao, F.-J. Crystal structure of tris(2,2′-bipyridine)cobalt(II) diperchlorate, $[Co(C_{10}H_8N_2)_3][ClO_4]_2$. *Z. Kristallogr.-N. Cryst. Struct.* **2005**, *220*, 483–484. https://doi.org/10.1524/ncrs.2005.220.14.503.
77. Batten, S.R.; Murray, K.S.; Sinclair, N.J. Tris(2,2′-bipyridyl-N,N')iron(II) diperchlorate. *Acta Cryst.* **2000**, *C56*, e320. https://doi.org/10.1107/S0108270100009185.
78. Zhou, Y.; Li, X.; Xu, Y.; Cao, R.; Hong, M. Tris(2,2′-bipyridine)nickel(II) diperchlorate. *Acta Cryst.* **2003**, *E59*, m300–m302. https://doi.org/10.1107/S1600536803008778.
79. Sangeeta, S. Tris(2,2′-bipyridine)nickel(ii) diperchlorate. *CSD Commun.* **2017**. https://doi.org/10.5517/ccdc.csd.cc1nw972.
80. Kawamata, Y.; Vantourout, J.C.; Hickey, D.P.; Bai, P.; Chen, L.; Hou, Q.; Qiao, W.; Barman, K.; Edwards, M.A.; Garrido-Castro, A.F.; et al. Electrochemically Driven, Ni-Catalyzed Aryl Amination: Scope, Mechanism, and Applications. *J. Am. Chem. Soc.* **2019**, *141*, 6392–6402. https://doi.org/10.1021/jacs.9b01886.
81. Pointillart, F.; Train, C.; Villain, F.; dit Moulin, C.C.; Gredin, P.; Chamoreau, L.-M.; Gruselle, M.; Aullon, G.; Alvarez, S.; Verdaguer, M. Six-fold Oxygen-Coordinated Triplet (S = 1) Palladium(II) Moieties Templated by Tris(bipyridine)ruthenium(II) Ions. *J. Am. Chem. Soc.* **2007**, *129*, 1327–1334. https://doi.org/10.1021/ja066817v.
82. Chesnut, D.J.; Haushalter, R.C.; Zubieta, J. The hydrothermal synthesis and structural characterization of a new class of compounds: Nickel organoamine-halocadmates. *Inorg. Chim. Acta* **1999**, *292*, 41–51. https://doi.org/10.1016/S0020-1693(99)00168-1.

83. Lin, S.-H.; Wang, Z.-K.; Zhang, B.-H.; Hu, H.-M.; Huang, J.-S. Crystal structure of tris(2,2′-bipyridine)nickel(II) tetrachlorozincate. *Jiegou Huaxue* **2000**, *19*, 95–98.
84. Eckenhoff, W.T.; Biernesser, A.B.; Pintauer, T. Structural characterization and investigation of iron(III) complexes with nitrogen and phosphorus based ligands in atom transfer radical addition (ATRA). *Inorg. Chim. Acta* **2012**, *382*, 84–95. https://doi.org/10.1016/j.ica.2011.10.016.
85. Dorval, C.; Tricoire, M.; Begouin, J.-M.; Gandon, V.; Gosmini, C. Cobalt-Catalyzed C(sp^2)–CN Bond Activation: Cross-Electrophile Coupling for Biaryl Formation and Mechanistic Insight. *ACS Catal.* **2020**, *10*, 12819–12827. https://doi.org/10.1021/acscatal.0c03903.
86. Ariyananda, L.M.D.; Norman, R.E. Tris(2,2′-bipyridyl-N,N')iron(II) bis[tetrachloroferrate(III)]. *Acta Crystallogr. Sect. E* **2002**, *58*, m775–m776. https://doi.org/10.1107/S1600536802021773.
87. Breu, J.; Zwicknagel, A. Chirale Erkennung bei Tris(diimin)-Metallkomplexen, 10 [1]. Vergleich der intermolekularen Wechselwirkungs- und Packungsmuster in der Reihe $[Cr(bpy)_3]^{n+}(PF_6)_n$ (n = 0–3). *Z. Naturforsch. B* **2004**, *59*, 1015–1025. https://doi.org/10.1515/znb-2004-0911.